AGU PUBLICATIONS

Geophysical Research Letters

RESEARCH LETTER
10.1002/2014GL062598

Key Points:
- Ionospheric Langmuir turbulence is generated by suprathermal electrons
- The suprathermal electrons are generated locally in the ionosphere
- The generation mechanism for the electrons is not yet understood

Correspondence to:
H. Akbari,
hakbari@bu.edu

Citation:
Akbari, H., J. L. Semeter, M. A. Hirsch, P. Guio, and M. J. Nicolls (2015), Evidence for generation of unstable suprathermal electron population in the auroral *F* region, *Geophys. Res. Lett.*, *42*, 185–192, doi:10.1002/2014GL062598.

Received 20 NOV 2014
Accepted 30 DEC 2014
Accepted article online 7 JAN 2015
Published online 23 JAN 2015

Evidence for generation of unstable suprathermal electron population in the auroral *F* region

H. Akbari[1], J. L. Semeter[1], M. A. Hirsch[1], P. Guio[2], and M. J. Nicolls[3]

[1]Department of Electrical and Computer Engineering and Center for Space Physics, Boston University, Boston, Massachusetts, USA, [2]University College London, London, UK, [3]SRI International, Menlo Park, California, USA

Abstract Anomalous incoherent scatter radar (ISR) spectra confined to narrow altitude ranges near the *F* region peak and correlated with dynamic auroral precipitation have previously been identified and explained in terms of the cavitating beam-driven Langmuir turbulence. In this work we used a one-dimensional Zakharov simulation to constrain the range of physical mechanisms underlying these observational features. We find that although Langmuir wave collapse and caviton formation generated by electron beams with energies of 1 keV can give rise to similar radar echoes, the predicted spectral features and intensities of such echoes are inconsistent with experimental data acquired by various ISRs. Our results suggest that the free energy for the turbulence must be provided by unstable low-energy ($5-20$ eV) electron populations and that such populations must be produced locally in the *F* region ionosphere.

1. Introduction

Recently, *Akbari et al.* [2012] and *Isham et al.* [2012] presented incoherent scatter radar (ISR) observations of strong echoes from the *F* region ionosphere. Spectral features of the observations (i.e., enhanced ion acoustic shoulders, zero-Doppler peak in the ion line channel, double-peaked spectra in plasma line channels) were interpreted in terms of signature of strong Langmuir turbulence and wave collapse. Langmuir turbulence has been the subject of many studies in the context of solar wind measurements [*Thejappa et al.*, 1999, 2012a, 2012b; *Graham et al.*, 2012a, 2012b; *Graham and Cairns*, 2013]. The recent observations of echoes by various incoherent scatter radars [*Schlatter et al.*, 2013; *Ekeberg et al.*, 2012; *Michell and Samara*, 2010] have attracted attention to this topic in the ionosphere as well.

The radar echoes are consistently observed in thin layers at or close to the *F* region peak [*Akbari et al.*, 2013; *Ekeberg et al.*, 2012; *Schlatter et al.*, 2013] and seem to be correlated with detections of one type of natural electromagnetic emission (Medium Frequency Burst) on the ground [*Akbari et al.*, 2013]. Among many interesting issues that need to be discussed is the source of free energy for the underlying turbulence. Typically, magnetospheric electron beams are assumed to be directly responsible for high-frequency ionospheric turbulence and their signatures in radar data. The electrons are assumed to be accelerated at much higher altitudes (~6000 km) and propagate downward to the observation altitudes, interacting with the ionospheric plasma along the way. Observations of the radar echoes on the edge of auroral arcs and just outside of regions of energetic electron precipitations [*Akbari et al.*, 2013] relate the echoes and the underlying turbulence to soft (<1 keV) electron precipitations. More accurate estimation of beam parameters—i.e., electron number density, mean energy, and velocity spread—however, requires simulation studies.

Observation of plasma waves by ISRs provides a way to accurately determine the phase velocity of the waves and therefore the energy of the electrons that may directly exchange energy with them. Assuming a background plasma density of $n = 2 \times 10^{11}$ m^{-3}, this energy is ~5 eV for Langmuir waves that are observed by the 450 MHz Poker Flat Incoherent Scatter Radar (with the detecting wave number, $k \sim 19$ m^{-1}) and increases as the density increases. Therefore, it is sometimes argued that the free energy for the turbulence must be provided by such low-energy electrons. For instance, by the secondary electrons that are produced as a result of collisional interaction of a primary high-energy beam and the background atmosphere.

Such an input energy source is plausible, and, in fact, required, if the turbulence and thus the echoes are produced by the parametric decay instability (PDI) at the corresponding wave numbers; however, it is not necessarily required if the turbulence is produced as a result of cavitating Langmuir turbulence and wave collapse. In the latter case, the input energy can be injected at lower wave numbers via noncollisional

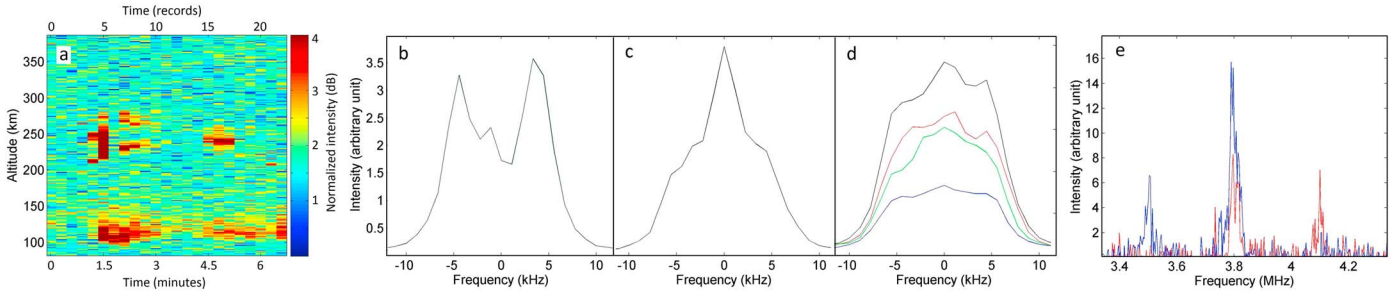

Figure 1. (a) Ion line range-time-intensity (RTI) plot derived from a separate 1 baud length pulse that accompanied AC. The time axis is shown in minutes as well as in 16 s intervals (records) starting at 6:04:35 (UT). Coherent echoes are originating from thin layers close to the *F* region peak (~250 km). (b–d) Examples of ion line spectra measured from the turbulence layers. Each spectrum, including those with different colors in Figure 1d, corresponds to different times. (e) Up- (blue) and down-shifted (red) plasma line spectra produced by long-pulse measurements for record 16 in Figure 1a. The spectra are averaged over a 70 km range gate centered at 290 km.

interaction of a primary electron beam with energy of hundreds of eV with the background *F* region plasma and subsequently transfer to higher wave numbers and be detected by ISRs. Any attempt to identify the source mechanism for the observed turbulence must consider carefully the regime of the Langmuir turbulence.

In this work we employ a one-dimensional Zakharov simulation to investigate the parameter regimes that will produce the ISR echoes and gain insight into the energy input mechanism. To this end, we simulate Langmuir turbulence produced by many different sets of beam parameters at the *F* region of the ionosphere. To distinguish between signatures of weak turbulence interactions, like the PDI, and strong turbulence interactions, like cavitons collapse, at the Poker Flat Incoherent Scatter Radar (PFISR) detecting wave number, we make sure that the injection of energy by the positive slope of the electron beams happens entirely at $k \ll 19\,\mathrm{m}^{-1}$. By applying this condition, we ensure that wave products of the PDI are entirely below the radar-detecting wave number, since the PDI only transfers energy from the injection wave number to lower wave numbers. Such waves are, therefore, invisible to the PFISR, and any wave enhancements at the radar-detecting wave number will be due to other processes, such as caviton formation.

2. Experimental Data

The experimental data presented here were obtained with the PFISR on 28 September 2011. The data include ion and plasma line measurements from a 480 μs long pulse as well as ion line measurements from a 16 baud alternating code (AC). The data were averaged and recorded in 16 s intervals (records). During each record, 96 radar pulses were sent every ~0.17 s. Figure 1a shows an ion line range-time-intensity (RTI) plot produced from a separate 1 baud length pulse that was added to the AC pulses. In this plot, in addition to incoherent scatter from the enhanced *E* region ionization (the enhancements below 150 km) due to energetic electron precipitation, coherent echoes are also present in thin layers close to the *F* region peak at ~250 km. These latter echoes are produced by scattering from ion density perturbations involved in Langmuir turbulence [*Akbari et al.*, 2012, 2013; *Isham et al.*, 2012]. Localization of the turbulence in thin layers has been previously explained in terms of the background electron density profile [*Akbari et al.*, 2013]. It is argued that field-aligned propagation of Langmuir waves in the presence of density gradient causes a change in the phase velocity of the waves that eventually leads to detuning the waves from the unstable electron population, limiting the amplification of the waves. Such effects are minimal at the *F* region peak due to the negligible vertical electron density gradient, resulting the vertical localization of the turbulence.

Figures 1b–1d show a few examples of ion line spectra obtained from turbulence layers. Figure 1b (averaged over 32 radar pulses, i.e., ~5.5 s) shows an enhanced double-humped spectrum where the peaks are located at the frequency of ion acoustic waves. The spectrum in Figure 1c measured 11 s later (again averaged over 32 radar pulses) shows a strong central peak at zero frequency. Signs of weaker enhancements at the frequency of ion acoustic waves are also present in this panel. If the spectrum was produced by averaging over 96 pulses, i.e., an entire 16 s record that includes Figures 1b and 1c, the result would look like the spectra shown in Figure 1d. The superposition of the two ion acoustic shoulders and the central peak would result in a flat spectrum that extends from the down-shifted shoulder to the up-shifted shoulder. This kind of flat spectrum has been previously observed by different ISRs [*Ekeberg et al.*, 2010; *Michell and Samara*, 2010; *Akbari et al.*, 2012, 2013].

Observation of a strong central peak in the ion line spectrum is commonly attributed to the existence of stationary density cavities produced by strong Langmuir turbulence [*DuBois et al.*, 1993a, 1993b], whereas the enhanced peaks seen in Figure 1b are attributed to enhanced level of ion acoustic waves that follow the linear dispersion relation. The flat spectra seen in Figure 1d, on the other hand, are not fully understood. The only speculation thus far is that the flat shape arises as a result of superposition of enhanced ion acoustic peaks and a strong central peak. Other experiments by European Incoherent Scatter (EISCAT) UHF and VHF radars have measured triple-peaked spectra in which the two ion acoustic shoulders and a distinct and equally enhanced central peak are present simultaneously [*Isham et al.*, 2012; *Schlatter et al.*, 2013].

Nonlinear features exist in the plasma line spectral measurements as well. Figure 1e shows the up- (blue) and down-shifted (red) plasma line spectra produced by the long-pulse measurements for record 16 in Figure 1a. The spectra are averaged over a 70 km range gate centered at 290 km. The up-shifted channel consists of a peak at 3.8 MHz and a peak at ~3.5 MHz, while the down-shifted channel consists of a peak at 3.8 MHz and a peak at ~4.1 MHz. The spectra for lower altitudes (at 250 and 210 km) only consist of the peaks at 3.8 MHz. The 3.8 MHz peaks commonly exist at other records in Figure 1a, where coherent echoes are seen in the corresponding ion line channel. However, the peaks at 3.5 and 4.1 MHz only exist in records 16 and 10. For record 10 where the echoes have almost disappeared in the ion line channel, the plasma line spectra still show the peaks at 3.8 MHz as well as the peak ~3.5 MHz in the up-shifted channel; however, the peak at ~4.1 MHz in the down-shifted channel is absent. In addition to these features, weak signs of double-peaked spectra similar to those discussed by *Akbari et al.* [2012] are seen in records 7–9 in the up-shifted channel but are not pronounced in the down-shifted channel. In all of the five records which plasma lines were enhanced, the enhancements were relatively more pronounced in the up-shifted channel.

3. Simulations

In order to gain insight into the source mechanism underlying such radar echoes, we employ one-dimensional Zakharov simulations. The Zakharov equations are fluid equations that describe the interaction of a high-frequency electric field and low-frequency ion density perturbations [*Zakharov*, 1972]. The source for the turbulence is included by a damping term that includes inverse Landau damping induced by the positive slope of the one-dimensional electron distribution function. The use of one-dimensional simulations in this work is justifiable base on in situ observations of beam-generated Langmuir turbulence in the topside auroral ionosphere where the measurements have shown that the generated waves dominantly propagate with angles less than 10° from the direction of the beam [*Newman et al.*, 1994].

For the simulations, we consider a 100 m long uniform plasma with typical parameters of the *F* region peak [*Guio and Forme*, 2006]. These are electron temperature $T_e = 3000$ K°, ion temperature $T_i = 1000$ K°, electron density $n_0 = 5 \times 10^{11}$ m^{-3}, electron-neutral collision frequency $\nu_{ec} = 100$ s^{-1}, and ion-neutral collision frequency $\nu_{ic} = 1$ s^{-1}, and we assume that the plasma only consists of atomic oxygen ions. The parameter range that we studied for the source electron beams are electron number density ratio $10^{-7} \leq \frac{n_b}{n_0} \leq 2.5 \times 10^{-5}$, average beam energy 100 eV $\leq E_b \leq$ 1 keV, and beam velocity spread $\Delta v_b = 0.3\ v_b$. Here n_b, m_e, and v_b are beam electron number density, electron mass, and the average beam velocity, respectively. Note that the combined electron distribution function that includes background electrons and beam electrons remains fixed for each simulation during the entire run time, and no quasi-linear diffusion or collisional modifications on the distribution function are included in our simulations. For further details on the simulation setup, readers are referred to *Guio and Forme* [2006]. The upper bound for the average beam energy has been chosen with regard to the fact that the radar echoes are found to be correlated with soft electron precipitations and the lower bound has been chosen with regard to the observation altitudes (~250 km). Precipitating electrons with yet lower energies will be collisionally stopped at higher altitudes and cannot reach the observation altitudes [*Fang et al.*, 2008].

Figure 2 shows the result of the simulation for one set of beam parameters ($\frac{n_b}{n_0} = 0.9 \times 10^{-5}$ and $E_b = 500$ eV). Figures 2a and 2b show the evolution of the electric field (*E*) and the ion density perturbations (*n*), respectively, as a function of time and wave number. The source electron beam initially enhances Langmuir waves with wave numbers $k \sim 4$ m^{-1} that satisfy the resonant condition $v_b \approx \omega_p/k$ (where ω_p is the plasma frequency). The positive or negative sign for wave numbers determines the propagation direction of the waves. The

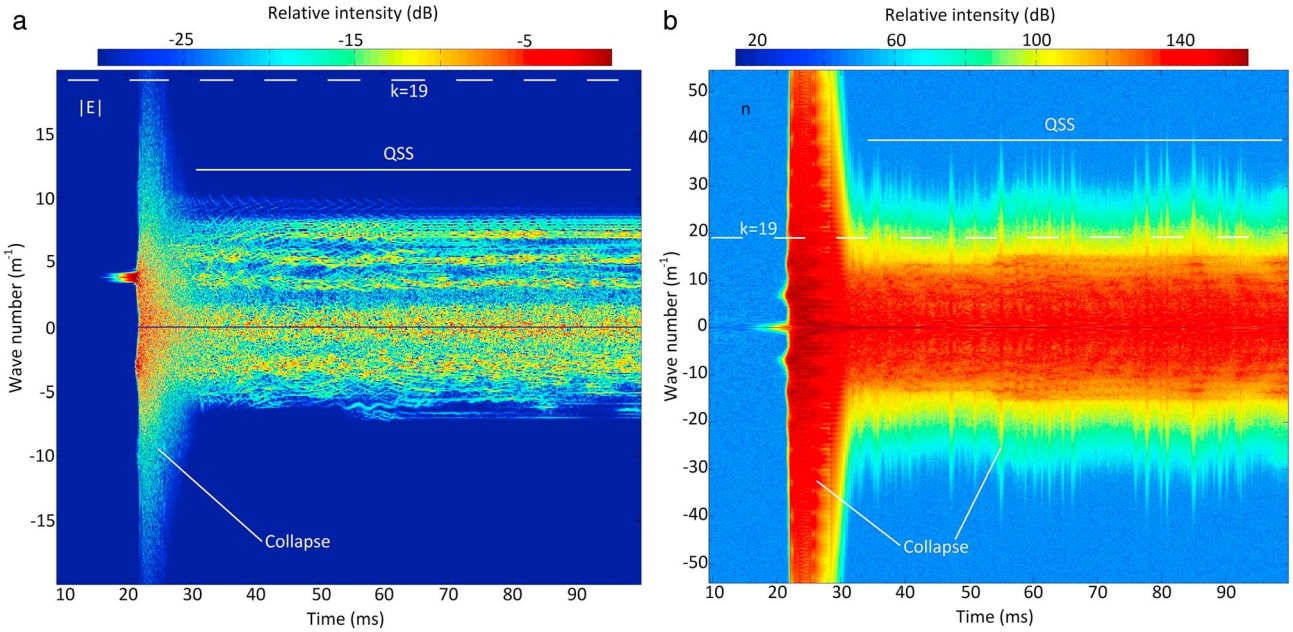

Figure 2. Evolutions of the (a) electric field magnitude and (b) ion density perturbations as a function of time and wave number. The electron beam has been applied at time $t = 0$ ms. White dashed lines show the PFISR detecting wave number.

asymmetric enhancement at $t < 22$ ms in the electric field spectrum, therefore, means that only Langmuir waves propagating in the direction of the electron beam are enhanced.

The dynamics of the turbulence depend on many factors, such as wave growth rate, wave number, frequency bandwidth, and the level of background density perturbations. Typically, once the waves grow to intensities higher than the parametric decay instability (PDI) threshold, a series of consecutive decays transfers the energy to lower wave numbers, during which ion acoustic waves and counterstreaming daughter Langmuir waves are generated. Once the energy reaches to the condensate ($k = 0$), the modulational instability may take over where the Langmuir waves with long wavelength become modulated and break up into smaller-scale wave packets accompanied by corresponding density wells [*Zakharov*, 1972]. However, consecutive PDIs can be truncated by direct nucleation of Langmuir energy into existing density depressions, and small-scale wave packets may form before energy transfers to the condensate [*Nicholson and Goldman*, 1978]. Our simulation results (not shown here) show that this nucleation mechanism is the process that happens in Figure 2 where Langmuir energy nucleates in the density depressions of ion acoustic waves that are produced after the first PDI at $t \sim 22$ ms. These results and the details of the interactions for many beam parameters will be presented in a separate paper. For the present work, we focus on the later stage of the turbulence when a quasi steady state has been reached.

If the intensity of a Langmuir packet is high enough, collapse initiates, i.e., the ponderomotive force of the high-frequency field pushes the plasma out of the corresponding density well, the initial wave packet narrows and becomes more intense, and the density well deepens. The signature of many simultaneous collapse events is seen in Figure 2 as the sudden transfer of energy to high wave numbers at $t \sim 22 - 28$ ms. At small scales, tens of λ_D (where λ_D is the Debye length), the collapsing wave packet experiences strong Landau damping [*Robinson*, 1997, and references therein], and the electric field dissipates leaving the density cavity unsupported by a ponderomotive force. The cavity then slowly relaxes, or breaks up, into ion sound pulses that continue to propagate in the system [*Doolen et al.*, 1985; *Robinson*, 1997].

After multiple collapse events, the level of ion density fluctuations increases, direct interaction of the beam and plasma weakens, and the number of collapse events decreases. From this point forward a quasi steady state (labeled "QSS") is reached where the turbulence is dominated by existence of coherent wave packets trapped into stationary density fluctuations, although linear Langmuir waves and ion acoustic waves also exist in the system. In quasi steady state the coherent wave packets can accumulate energy from the background turbulence and go through the cycle of nucleation-collapse-dissipation [*Doolen et al.*, 1985].

In the example shown in Figure 2b, such collapse events are visible, although much less frequent and intense than those in the initial stage of the turbulence. Note that the collapse signature is not seen in the electric field plot due to the intensity scale chosen for this plot.

4. Comparison With Experimental Evidence

4.1. Beam Electron Number Density

Repeating the simulation for over 100 beams that explore the parameter ranges mentioned above reveals that in order for the PFISR to observe the cavitating Langmuir turbulence, an electron number density ratio of $\frac{n_b}{n_0} \geq 10^{-5}$ is typically required. For electron number density ratios much larger than the criteria mentioned above, the instability develops over relatively short time scales. For instance, if the electron number density ratio for the simulation shown above is increased to $\frac{n_b}{n_0} = 1.5 \times 10^{-5}$, the instability fully develops in only ~8 ms. Within such short time scales, saturation effects due to propagation of the Langmuir waves in the background density gradient is negligible, and the theory proposed by *Akbari et al.* [2013] to explain the localization of the echoes in thin layers is not applicable. We therefore conclude that if the radar echoes are produced by cavitating Langmuir turbulence, generated by electron beams streaming from higher altitudes, and localized in thin layers at the *F* region peak, due to propagation effects, the electron number density of the source beams may not be much higher or lower than $n_b \approx n_0 \times 10^{-5}$.

4.2. ISR Detecting Wave Number

Figure 2 presents an important point on the wave number dependence of the turbulence. It is seen that once we pass the initial stage of the turbulence at $t \sim 22 - 28$ ms, the turbulence in quasi steady state is highly k dependent. In Figure 2b the main portion of the density perturbations exists at low wave numbers ($k < 15\ \mathrm{m}^{-1}$). For higher wave numbers ($15 < k < 30\ \mathrm{m}^{-1}$) the level of density fluctuations drops by orders of magnitude below the level for $k < 15\ \mathrm{m}^{-1}$. This level of density fluctuations, however, is still orders of magnitude above the thermal level. The observed wave number dependence can be easily explained. Intense ion density perturbations at $k < 15\ \mathrm{m}^{-1}$ are produced by a cascade of PDIs which efficiently transfers energy form the upper bound ($k = 15\ \mathrm{m}^{-1}$) to small wave numbers ($k \approx 0\ \mathrm{m}^{-1}$). The PDI do not transfer any energy to higher wave numbers; however, a small portion of energy in the range $k < 15\ \mathrm{m}^{-1}$ can still leak to $k > 15\ \mathrm{m}^{-1}$ via two other processes, and these are (1) wave collapse and (2) a two-step process by which first, high-frequency waves are produced by scattering of Langmuir waves off ions, and second, the produced high-frequency waves decay to produce ion density perturbation at $k > 15\ \mathrm{m}^{-1}$. Both these processes are secondary relative to the PDI, and thus, the generated waves in the range $15 < k < 30\ \mathrm{m}^{-1}$ are orders of magnitude weaker than those in the range $k < 15\ \mathrm{m}^{-1}$.

The point of the discussion above is that if the turbulence is generated by injection of energy at low wave numbers and is brought to higher wave numbers by wave collapse or scattering off ions, upon being detected by various ISRs such as the EISCAT VHF (detecting wave number $k \sim 11\ \mathrm{m}^{-1}$), the PFISR (detecting wave number $k \sim 19\ \mathrm{m}^{-1}$), and the EISCAT UHF (detecting wave number $k \sim 38\ \mathrm{m}^{-1}$) would produce backscatters that are orders of magnitude different in intensity in the three radars. This is in clear disagreement with the observations, where the intensity of the echoes in the three ISRs are similarly 15–20 dB above the thermal level [*Isham et al.*, 2012; *Akbari et al.*, 2012; *Schlatter et al.*, 2013]. We therefore conclude that the injection of energy to the system should happen, at least in part, at high wave numbers. This in turn requires low-energy electrons of the order $5 - 20$ eV.

4.3. Ion Line Spectral Morphology

Further discrepancy between experimental observations and the hypothesis that the beam energy injection happens at small wave numbers (long wavelengths) appears in spectral features of density perturbations. It is seen in our simulations that the behavior of density cavities after the dissipation stage and the level of ion acoustic density pulses emitted from them strongly depends on the damping rate for density fluctuations which, in turn, depends on the electron to ion temperature ratio. For the temperature ratio of $\frac{T_e}{T_i} = 3$ (plausible for the auroral *F* region), it is seen that the density cavities slowly relax in place rather than emitting strong sound pulses. The stationary density cavities then dominantly give rise to a strong central peak at zero frequency in ISR's ion line channel with no strong ion acoustic sidebands. This picture changes if we

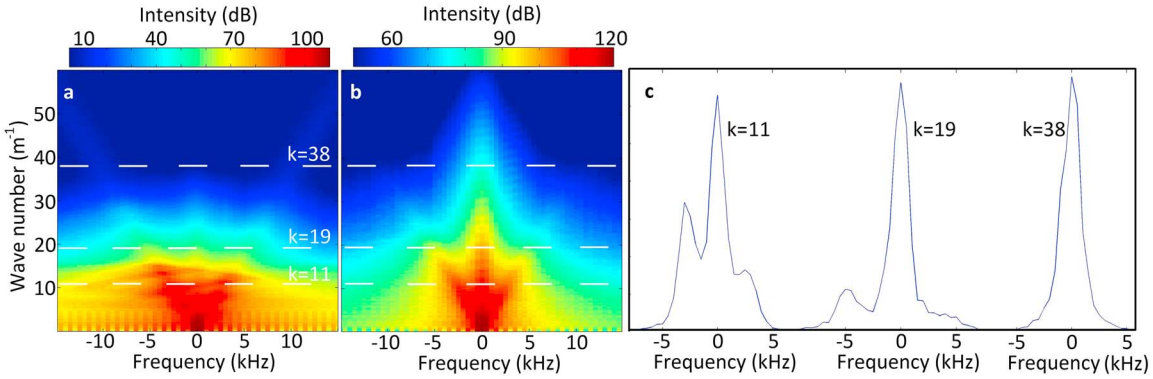

Figure 3. (a) The averaged frequency behavior of density perturbations in Figure 2b once the quasi steady state has been reached. (b) Similar to Figure 3a but for a simulation run with a higher input energy to the system. (c) Horizontal cuts through Figure 3b at wave numbers 11, 19, and 38 m^{-1} (shown by white dashed lines in Figures 3a and 3b), modeling the spectra that would be obtained if the turbulence was detected by the EISCAT VHF, PFISR, and the EISCAT UHF radars, respectively.

decrease the ion acoustic damping rate by using a higher temperature ratio. In this case, first, following the dissipation stage unsupported density cavities break into ion sound pulses, and second, the reduced damping enables the ion sound pulses to continue to propagate for a longer time in the system giving rise to resonant ion acoustic shoulders.

The dominance of a zero-frequency central peak in the ion line spectra is shown in Figure 3. Figure 3a shows the averaged frequency behavior of density perturbations in Figure 2b once the system has reached the quasi steady state. The enhancements produced by Langmuir decay follow the linear dispersion relation $\omega = C_s|k|$ where ω, C_s, and k are wave frequency, sound speed, and wave number. A very weak central peak at zero frequency is also observed for $k < 20\,m^{-1}$ that is the signature of the sporadic collapse events seen in Figure 2b. No density perturbations above thermal level is seen above $k = 35\,m^{-1}$. Increasing the input energy to the system, by increasing the beam number density from $\frac{n_b}{n_0} = 0.9\times10^{-5}$ to $\frac{n_b}{n_0} = 1.5\times10^{-5}$, results in an increase in the number of collapse events, and consequently, a pronounced central peak appears in the frequency spectrum. This is shown in Figure 3b where the central peak dominates the shape of the spectrum at higher wave numbers. In Figure 3c we plot the ion line spectra that would be seen if the turbulence was detected by the EISCAT VHF, PFISR, and the EISCAT UHF radars. These are horizontal cuts through Figure 3b since ISRs observe wave activities at single wave numbers.

The spectrum at $k = 38\,m^{-1}$ is dominated by a single central peak, and no resonant ion acoustic peaks similar to those seen by the EISCAT UHF radar [*Schlatter et al.*, 2013] are seen. We therefore propose the possibility that the observed enhanced ion acoustic peaks in the EISCAT UHF radar measurements are produced by the parametric decay instability at the corresponding wave numbers. This, in turn, requires the existence of lower energy electrons ($E_b < 20$ eV) at the observations altitudes, and since such electrons cannot propagate from higher altitudes, this population should be produced locally.

Secondary electrons produced as a result of collisional interaction of primary energetic electrons with neutral atmosphere have been previously suggested to provide free energy for some *E* region Langmuir wave enhancements [*Valladares et al.*, 1988; *Kirkwood et al.*, 1995] as well as two *E* region plasma instabilities involving modes that propagate close to perpendicular to the magnetic field [*Basu et al.*, 1982; *Jasperse et al.*, 2013]. However, given their pitch angle distribution, it is yet to be determined whether such secondary electrons would develop the intense unstable feature that is required to initiate the PDI, namely, a strong positive slope in their one-dimensional distribution function.

4.4. Plasma Line Measurements

The presence of additional wave activity is strongly suggested by the observation of the asymmetric double-peaked plasma line measurements shown in Figure 1e. In Figure 1e the peaks at 3.8 MHz in both up- and down-shifted channels exist at lower altitudes and also in other records, and therefore, we assume that these peaks are due to Langmuir turbulence. It is the two extra peaks at 4.1 and 3.5 MHz that require explanation. The frequency offset of ~ −300 kHz of the secondary peak with respect to the main peak in the

up-shifted channel, and the matching positive frequency offset in the down-shifted channel, confirm that the peaks are not produced as a result of spatial/temporal averaging and suggests that the peaks are produced by nonlinear interactions between Langmuir waves and a secondary wave. A variety of electrostatic and electromagnetic modes exists and has been observed in the ionosphere during disturbed periods [*André*, 1997; *LaBelle and Treumann*, 2002; *Samara and LaBelle*, 2006]. Determining which of these modes are responsible for the asymmetric spectra presented here would also provide further insights into source mechanisms for ionospheric turbulence.

5. Summary

We have used a one-dimensional Zakharov simulation to investigate the beam-generated Langmuir turbulence in the auroral ionosphere. We have found the following:

1. Simultaneous enhancements in ion line and plasma line channels of the PFISR can be produced by strong Langmuir turbulence and caviton collapse generated by relatively strong ($n_b \sim n_0 \times 10^{-5}$) soft electron beams ($100\,\mathrm{eV} \leq E_b \leq 1\,\mathrm{keV}$).
2. Turbulence developed by injection of energy to small wave numbers and transferred to higher wave numbers by caviton collapse or scattering off ions, upon being detected by ISRs with different detecting wave numbers, would result in radar backscatter echoes that are orders of magnitude different in intensity. This is in clear disagreement with the experimental observations, suggesting that at least a portion of the energy is provided at higher wave numbers by a locally generated suprathermal electron population in the 5–20 eV range.
3. At high wave numbers such as $k = 38\,\mathrm{m}^{-1}$, i.e., detecting wave number of the EISCAT UHF radar, caviton collapse would give rise to a dominant zero-frequency peak in the ion line channel which does not match the experimental data. Observations of enhanced ion acoustic peaks, therefore, suggest that the PDI operates at the observations wave numbers. This in turn requires local energization of lower energy electrons ($E_b < 20\,\mathrm{eV}$) at ~250 km.
4. Lack of success in simulating the flat ion line spectra suggests that processes and wave modes other than those included in Zakharov model may be present and affect ionospheric turbulence.
5. The existence of other modes and processes is also supported by observations of nonlinear features in the plasma line measurements.

We realize that the available data are not sufficient to confirm our explanation, but the mentioned scenario is argued as the most plausible. In short, we believe that the exact processes underlying the radar echoes are far from understood. The use of ISRs in collaboration with other common-volume sensors (i.e., optical imagers [*Semeter et al.*, 2005]) and employing more general simulations, like particle-in-cell simulations [*Diaz et al.*, 2010, 2011], may provide the necessary context to fully understand magnetosphere-ionosphere interactions at the finest scales in the geospace system.

Acknowledgments
This work was supported by the National Science Foundation under grants AGS-1244675 and AGS-1339500 and by the Air Force Office of Scientific Research under contract FA9550-12-1-018. The ISR data are accessible from the SRI International online database. For the simulation data, contact the first author of the paper.

The Editor thanks two anonymous reviewers for their assistance in evaluating this paper.

References

Akbari, H., J. L. Semeter, H. Dahlgren, M. Diaz, M. Zettergren, A. Strømme, M. J. Nicolls, and C. Heinselman (2012), Anomalous ISR echoes preceding auroral breakup: Evidence for strong Langmuir turbulence, *Geophys. Res. Lett.*, *39*, L03102, doi:10.1029/2011GL050288.

Akbari, H., J. L. Semeter, M. J. Nicolls, M. Broughton, and J. W. LaBelle (2013), Localization of auroral Langmuir turbulence in thin layers, *J. Geophys. Res. Space Physics*, *118*, 3576–3583, doi:10.1002/jgra.50314.

André, M. (1997), Wave and wave-particle interactions in the auroral region, *J. Atmos. Sol. Terr. Phys.*, *5914*, 1687–1712, doi:10.1016/S1364-6826(96)00173-3.

Basu, B., T. Chang, and J. R. Jasperse (1982), Electrostatic plasma instabilities in the daytime lower ionosphere, *Geophys. Res. Lett.*, *9*, 68–71, doi:10.1029/GL009i001p00068.

Diaz, M. A., J. L. Semeter, M. Oppenheim, and M. Zettergren (2010), Analysis of beam plasma instability effects on incoherent scatter spectra, *Ann. Geophys.*, *28*, 2169–2175, doi:10.5194/angeo-28-2169-2010.

Diaz, M. A., M. Oppenheim, J. L. Semeter, and M. Zettergren (2011), Particle-in-cell simulation of incoherent scatter radar spectral distortions related to beam-plasma interactions in the auroral ionosphere, *J. Geophys. Res.*, *116*, A00K10, doi:10.1029/2010JA016096.

Doolen, G. D., D. F. DuBois, and H. A. Rose (1985), Nucleation of cavitons in strong Langmuir turbulence, *Phys. Rev. Lett.*, *54*, 804, doi:10.1103/PhysRevLett.54.804.

DuBois, D. F., A. Hanssen, H. A. Rose, and D. Russell (1993a), Space and time distribution of HF excited Langmuir turbulence in the ionosphere: Comparison of theory and experiment, *J. Geophys. Res.*, *98*(A10), 17,543–17,567, doi:10.1029/93JA01469.

DuBois, D. F., A. Hansen, H. A. Rose, and D. Russell (1993b), Excitation of strong Langmuir turbulence in the ionosphere: Comparison of theory and observations, *Phys. Fluids B*, *5*(7), 2616–2622, doi:10.1063/1.860699.

Ekeberg, J., G. Wannberg, L. Eliasson, and K. Stasiewicz (2010), Ion-acoustic solitary waves and spectrally uniform scattering cross section enhancements, *Ann. Geophys.*, *28*, 1299–1306, doi:10.5194/angeo-28-1299-2010.

Ekeberg, J., G. Wannberg, L. Eliasson, and I. Häggström (2012), Soliton-induced spectrally uniform ion line power enhancements at the ionospheric F region peak, *Earth Planets Space*, *64*, 605–611, doi:10.5047/eps.2012.02.005.

Fang, X., C. E. Randall, D. Lummerzheim, S. C. Solomon, M. J. Mills, D. R. Marsh, C. H. Jackman, W. Wang, and G. Lu (2008), Electron impact ionization: A new parameterization for 100 eV to 1 MeV electrons, *J. Geophys. Res.*, *113*, A09311, doi:10.1029/2008JA013384.

Graham, D. B., and I. H. Cairns (2013), Electrostatic decay of Langmuir/z-mode waves in type III solar radio bursts, *J. Geophys. Res. Space Physics*, *118*, 3968–3984, doi:10.1002/jgra.50402.

Graham, D. B., I. H. Cairns, D. R. Prabhakar, R. E. Ergun, D. M. Malaspina, S. D. Bale, K. Goetz, and P. J. Kellogg (2012a), Do Langmuir wave packets in the solar wind collapse?, *J. Geophys. Res.*, *117*, A09107, doi:10.1029/2012JA018033.

Graham, D. B., I. H. Cairns, D. M. Malaspina, and R. E. Ergun (2012b), Evidence against the oscillating two-stream instability and spatial collapse of Langmuir waves in solar Type III radio bursts, *Astrophys. J. Lett.*, *753*(1), L18, doi:10.1088/2041-8205/753/1/L18.

Guio, P., and F. Forme (2006), Zakharov simulations of Langmuir turbulence: Effects on the ion-acoustic waves in incoherent scattering, *Phys. Plasmas*, *13*, 122902, doi:10.1063/1.2402145.

Isham, B., M. T. Rietveld, P. Guio, F. R. E. Forme, T. Grydeland, and E. Mjolhus (2012), Cavitating Langmuir turbulence in the terrestrial aurora, *Phys. Rev. Lett.*, *108*, 105003, doi:10.1103/PhysRevLett.108.105003.

Jasperse, J. R., Basu, B., Retterer, J. M., Decker, D. T., and Chang, T. (2013), High frequency electrostatic plasma instabilities and turbulence layers in the lower ionosphere, in *Space Plasmas: Coupling Between Small and Medium Scale Processes*, edited by M. Ashour-Abdalla, T. Chang, and P. Dusenbery, AGU, Washington, D. C., doi:10.1029/GM086p0077.

Kirkwood, S., H. Nilsson, J. Lilensten, and M. Galand (1995), Strongly enhanced incoherent-scatter plasma lines in aurora, *J. Geophys. Res.*, *100*(A11), 21,343–21,355, doi:10.1029/95JA00765.

LaBelle, J., and R. A. Treumann (2002), Auroral radio emissions. 1. Hisses, roars, and bursts, *Space Sci. Rev.*, *101*, 295–440, doi:10.1023/A:1020850022070.

Michell, R. G., and M. Samara (2010), High-resolution observations of naturally enhanced ion acoustic lines and accompanying auroral fine structures, *J. Geophys. Res.*, *115*, A03310, doi:10.1029/2009JA014661.

Newman, D. L., M. V. Goldman, R. E. Ergun, and M. H. Boehm (1994), Langmuir turbulence in the auroral ionosphere: 1. linear theory, *J. Geophys. Res.*, *99*(A4), 6367–6376.

Nicholson, D. R., and M. V. Goldman (1978), Cascade and collapse of Langmuir waves in two dimensions, *Phys. Fluids*, *21*, 1766, doi:10.1063/1.862093.

Robinson, P. A. (1997), Non-linear wave collapse and strong turbulence, *Rev. Modern Phys.*, *69*, 507, doi:10.1103/RevModPhys.69.507.

Samara, M., and J. LaBelle (2006), Structured waves near the plasma frequency observed in three auroral rocket flights, *Ann. Geophys.*, *24*, 2911–2919, doi:10.5194/angeo-24-2911-2006.

Schlatter, N. M., N. Ivchenko, T. Sergienko, B. Gustavsson, and B. U. E. Brändström (2013), Enhanced EISCAT UHF backscatter during high-energy auroral electron precipitation, *Ann. Geophys.*, *31*, 1681–1687, doi:10.5194/angeo-31-1681-2013.

Semeter, J., C. Heinselman, G. G. Sivjee, H. U. Frey, and J. W. Bonnell (2005), Ionospheric response to wave-accelerated electrons at the poleward auroral boundary, *J. Geophys. Res.*, *110*, A11310, doi:10.1029/2005JA011226.

Thejappa, G., M. L. Goldstein, R. J. MacDowall, K. Papadopoulos, and R. G. Stone (1999), Evidence for Langmuir envelope solitons in solar type III burst source regions, *J. Geophys. Res.*, *104*(A12), 28,279–28,293, doi:10.1029/1999JA900363.

Thejappa, G., R. J. MacDowall, M. Bergamo, and K. Papadopoulos (2012a), Evidence for the oscillating two steam instability and spatial collapse of Langmuir waves in a solar type III radio burst, *Astrophys. J.*, *747*, L18, doi:10.1088/2041-8205/753/1/L18.

Thejappa, G., R. J. MacDowall, and M. Bergamo (2012b), In situ detection of strong Langmuir turbulence processes in solar type III radio bursts, *J. Geophys. Res.*, *117*, A08111, doi:10.1029/2012JA017695.

Valladares, C. E., M. C. Kelley, and J. F. Vickrey (1988), Plasma line observations in the auroral oval, *J. Geophys. Res.*, *93*(A3), 1997–2003, doi:10.1029/JA093iA03p01997.

Zakharov, V. E. (1972), Collapse of Langmuir waves, *Sov. J. Exp. Theor. Phys.*, *35*, 908–914.